

# Acoustic emission study on the effect of notch shape and temperature on elastic energy release during impact testing of 17Mn1Si pipe steel

S.V. Panin<sup>ab</sup> A.V. Byakov<sup>ab</sup> I.V. Vlasov<sup>ab</sup> P.O. Maruschak<sup>c</sup> F. Berto<sup>d</sup> A. Vinogradov<sup>de</sup>

## Abstract

Main fracture mechanisms are determined in 17Mn1Si steel during impact Charpy testing of specimens with three types of notches at different test temperatures covering ductile-to-brittle transition. The influence of the notch shape on the amount of expended mechanical energy (according to the loading diagram) and released elastic energy (according to the recorded acoustic emission signal) is analyzed. A combined application of fracture mechanics and acoustic emission methods is proven effective for better understanding of dynamic fracture and ductile-to-brittle transition from the viewpoint of energy-based approaches to crack initiation and propagation. It is suggested that the link between the AE signal and the ductile-to-brittle transition in dynamic loading can be established to develop a tool for in situ characterization of the fracture process.

## Keywords

Dynamic fracture

Ductile-to-brittle transition

Crack initiation

Crack propagation

Fractography

Fracture mechanisms

Acoustic emission

## 1. Introduction

The [acoustic emission](#) (AE) method has gained great popularity for in-situ monitoring and post-test analysis of the processes occurring during internal structural rearrangements underlying [plastic deformation](#) and fracture in a wide range of [structural materials](#) from pure metals to [alloys, steels](#), and composites [\[1\]](#), [\[2\]](#), [\[3\]](#). Due to its outstanding sensitivity to the onset of fracture, the AE method has been used to

estimate [fracture toughness](#) of different structural materials. The significance of AE measurements for the investigation of the behaviour of mechanical systems and structures under load has been documented in [great detail](#) in many comprehensive studies reviewing a broad scope of methodological aspects of AE acquisition and source location, signal processing, analysis and interpretation of results, which are applicable to [fracture mechanics](#) testing, see, for example, [\[4\]](#), [\[5\]](#), [\[6\]](#), [\[7\]](#), [\[8\]](#), [\[9\]](#), [\[10\]](#), [\[11\]](#), [\[12\]](#).

The determination of fracture mechanics characteristics by the AE method in the earlier studies was based primarily on [observable](#) changes in the slope of some AE parameters vs. fracture mechanics parameters such as [crack opening displacement](#) [\[13\]](#), [\[14\]](#), [stress intensity factor  \$K\$](#)  [\[15\]](#), [\[16\]](#), [\[17\]](#) or  $J$ -Integral [\[18\]](#), [\[19\]](#).

The reliable distinction between ductile and [brittle fracture](#) modes in the AE signal is of crucial importance for the successful application of this [method in fracture mechanics](#).

This distinction is made by [fracture surface](#) appearance post-mortem, while the chronology of fracture activation and [progression](#) is another [critical input](#) for either accurate [characterization](#) of [damage processes](#) or realistic modeling of the [fracture behavior](#). The appearance of signals with characteristic [amplitude](#) and frequency distributions was recognized as a promising indicator of different fracture modes. Ono and Yamamoto [\[20\]](#) demonstrated that different AE sources could be distinguished in A533B steels: (i) plastic deformation of the [ferrite matrix](#), giving rise to continuous acoustic emissions predominantly during yielding, and (ii) fracture events associated with deboning of [non-metallic inclusions](#), emitting burst-type signals with the [peak amplitude](#) distribution of a Weibull type.

Despite a broad variety of methods used with a different level of success, identifying unambiguous signatures of ductile and brittle fracture and a brittle-to-ductile transition by the AE technique in fracture mechanics testing is still challenging. Contradictory results have been reported in the literature. For example, Kostryzhev et al. [\[21\]](#) applied a wavelet transform to investigate fracture evolution during [impact testing](#) of high [strength steels](#). These authors associated a distinct low-frequency peak at about 50 kHz in the wavelet spectra with plastic deformation of [ferrite](#). The high-frequency peak in the range of 200–500 kHz was attributed to the transgranular cleavage of ferrite. As opposes to this Kietov et al. [\[22\]](#) have recently reported the results of AE investigations during [Charpy impact test](#) of [nodular cast iron](#). No AE signals generated by [mechanisms related](#) to plastic deformation and ductile [crack propagation](#) were detected, while local [cleavage fracture](#) was easily distinguished and the AE amplitude was correlated with the size of the cleavage areas. Tronskar et al. [\[23\]](#) applied the AE

method to determine the beginning of ductile tearing during impact fracture. The onset of [fracture initiation](#) and the crack propagation stage were successfully distinguished. The use of the [Fourier](#) transformation for AE signal processing revealed the characteristic phases and fracture modes based on the characteristic frequency and time of AE signals. The brittle fracture had characteristic peak amplitude frequencies in the 493–547 kHz range and a very short duration of the AE signals while ductile tearing occurred with [energy release](#) over a wide frequency range of 400–693 kHz (though overlapping with that from brittle fracture) and with significantly [longer duration](#). Using an amplitude and [frequency analysis](#) Chuluunbat et al. [24] identified AE signals related to plastic deformation, fracture initiation and [crack growth](#) in X70 [pipe steel](#). Conventional signal parameters were complemented by the spectral analysis of AE [waveforms](#) correlated with the load–displacement/load–time curves obtained during single edge-notched [tensile specimens](#) testing. It was shown that the [strain rate](#), test temperature, and the stress [concentrator](#) shape affect the AE behavior. However, it should be noticed that the [frequency bands](#) corresponding to signals generated by plastic deformation and crack growth were found significantly overlapping because void nucleation and [coalescence](#) in the ductile steel was mediated by plastic deformation. [Charpy impact toughness](#) tests are among the most widely used in routine industrial practice for express evaluation of [materials resistance](#) to [stress concentration](#), evaluation of impact toughness and [ductile-to-brittle transition temperature](#) [25]. The literature regarding the AE application to dynamic testing including Charpy impact testing is still scarce. Admittedly, [dynamic tests](#) are among most difficult for implementation of AE methods due to the [combined effects](#) of strikers, short time of testing, limited statistics of events, etc. However, the amplitude analysis of the AE signals obtained during impact testing of fatigue pre-cracked Charpy specimens of dual phase by Richter et al. [26] has shown the possibility to distinguish the time when the AE activity is dominated by plastic deformation during ductile [crack initiation](#) from that associated with [brittle crack](#) growth: low amplitude continuous AE was associated with plastic deformation while the high amplitude [transients](#) were considered due to brittle crack behavior. However, this consideration is simplified since the occurrence of appreciable plasticity in ductile materials could generate high amplitude AE bursts and may cause difficulty in correctly determining the fracture toughness [27]. The sensitivity of AE signals to the mode of fracture made it possible for Roy et al. [28] to compare the value of fracture toughness of four steels having different ductility. The valid ASTM [fracture toughness tests](#) were performed. By analyzing the cumulative energy, cumulative counts, and intensity of AE signals, the fracture initiation point was

determined with [good accuracy](#). The advent of instrumented [pendulum](#) impact testers [29] enabled recording and analyzing the [impact energy](#) curves to quantify the [energy expended](#) during crack initiation and propagation. As a result, the [fracture energy](#) can be estimated at each of these key stages. A large part of the [mechanical energy](#) imposed into the specimen is dissipated due to plastic deformation (as well as in the form of heat) during impact bending. The other part is released in the form of [elastic waves](#) which can be detected by [piezoelectric](#) AE [transducers](#).

Thus, based on data available to date, one can conclude that (i) AE is very sensitive to both extrinsic [loading conditions](#) (strain rate, stress concentration, temperature, etc.) and intrinsic microstructural [factors](#) ([phase](#) content, grain size, distribution of non-metallic inclusions, [dislocation density](#), etc.) governing the fracture behaviour under [dynamic loading](#); (ii) a plethora of methods for AE analysis has been proposed and tested in a number of studies on many structural materials, albeit with contrasting results so that no consensus still exists regarding the “best” (or even just “commonly accepted”) methods of AE acquisition and processing in [dynamic fracture mechanics](#) testing; (iii) due to its selective sensitivity to plastic deformation and fracture and the capacity to distinguish between these two processes, AE is well suited to shed some light on the ductile-to-brittle transition in steels.

The present work aims at reducing the deficit of AE data during dynamic testing in the temperature range covering the ductile-to-brittle transition. We endeavor to demonstrate that the features of the AE signal can be linked to the features of the ductile/brittle behavior of a typical commercial pipe steel during standard testing. An instrumented Charpy impact bending was used for [high strain rate](#) loading of ductile 17Mn1Si pipe steel specimens with three geometries of notches. The obtained results will be interpreted in terms of brittle/ductile fracture behavior in conjunction with the notch shape effect on the amount of expended mechanical energy (according to the loading curve) and the released [elastic energy](#)(according to the detected AE signal).

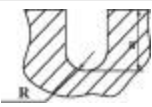
To avoid any possible losses associated with amplitude thresholding, a continuous waveform recording was implemented during the entire test commencing from the striker’s impact upon the specimen and ending with the specimen fracture into two parts. A methodology is proposed for the AE analysis guided by the features of the dynamic loading curve. The conventional temporal analysis of signals was complemented by the time-frequency analysis employing a continuous [wavelet decomposition](#).

## 2. Experimental procedure

[Mechanical impact](#) tests were conducted on the standard [Charpy](#) specimens cut by electric spark machining from commercial 30 mm thick [rolled sheet](#) steel 17Mn1Si. The stress concentrators were introduced in the form V-, U-, and I-shaped notches of 2 mm depth. The notch shape was varied to study its effect on the [fracture toughness](#) at each stage of [crack growth](#). The specimens for [impact testing](#) with U- and V-shape notches were fabricated following the ASTM E23-16b [30] guidelines. The [opening angle](#) for the V-shape notch was equal to 45°.

The specimens were tested at temperatures  $T = 20, -20, \text{ and } -60 \text{ }^\circ\text{C}$  on an Instron 450MPX [pendulum](#) impact tester equipped with an instrumented striker. The specimens were cooled in the Lauda RP 870 [chiller](#) during 10 min before testing. The time lag between the specimen removal from the cooling chamber and the impact did not exceed 5 s. The [dynamic loading](#) curve was recorded during each test. [Table 1](#) shows the notch geometries, dimensions and corresponding [stress concentration factors](#) (SCF). We should notice that the SCF factor is commonly used for estimating the stress–strain state at the [notch tip](#) during elastic loading in force-based models. Since the energy-based approach was adopted for discussion in the present work, this parameter is shown for reference only.

Table 1. Geometry of the notches and corresponding [stress concentration factors](#) in the 17Mn1Si steel specimens.

Notch shape	Geometrical shape	Notch tip radius, $R$ , mm	SCF	Notch depth, mm
U		1.0	2.1	2.0
V		0.25	3.44	
I		0.1	9.94	

The AE signal generated during impact fracture was detected by a broadband WD (Physical [Acoustics](#) Ltd, USA) [transducer](#) mounted on the tester support 0.5 m apart from the specimen. The acoustic signal was therefore attenuated so that the electric signal at the output of the transducer did not exceed the ADC [input range](#). Due to the high [amplitude](#) of the recorded acoustic signal, the AE transducer was connected directly to the ADC board Adlink PCI-9812 operating at a [sampling frequency](#) of 10 MHz in the range  $\pm 1 \text{ V}$ . All signals were normalized to the unit [peak amplitude](#).

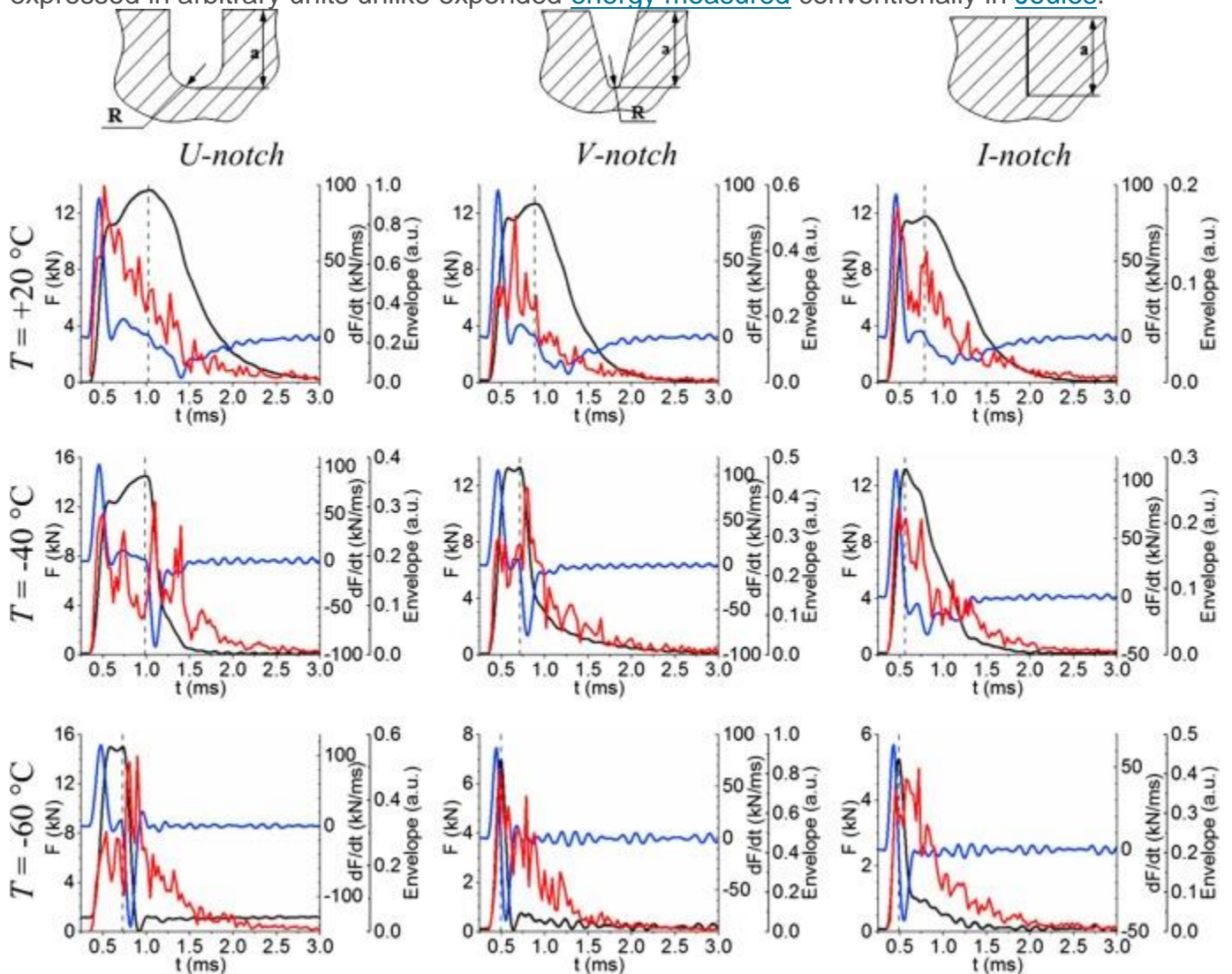
The continuous wavelet spectra were calculated in the frequency range from 50 to 500 kHz with a 5 kHz step using the free AGU-Vallen Wavelet software [31]. The released AE energy EAE was calculated in the time domain as the time integral of squared voltage over the signal duration. The envelope of the AE [signal recorded](#) continuously during impact fracture was obtained by the [Hilbert transform](#). It was then smoothed by a LOWESS (locally weighted least squares) procedure with a 20  $\mu$ s window.

The mechanisms and stages of impact fracture were considered in depth in our previous companion study [32] where detailed fractographic analysis was presented. Two characteristic stages were readily distinguished (I – [crack initiation](#) stage and II – [crack propagation](#) stage) by the analysis of the shape of the dynamic loading curve  $F(t)$  or, more precisely, of its derivative with respect to time  $dF/dt$ . They also can be recognized through characteristic changes in the AE signal as will be shown below. After impact testing, the [fracture surface](#) was examined by a [scanning electron microscope](#) (SEM) Leo EVO 50 (Carl Zeiss) in the secondary electron mode. The fracture surface was observed at the crack initiation point and at the center of the sample.

### 3. Results and discussion

[Fig. 1](#) shows the [impact toughness](#) curves of the specimens with different notches at different temperatures. The temperature plays a crucial role in [fracture toughness](#). It is of particular importance for the steels having a [body-centered cubic](#) (BCC) lattice. At high temperatures, BCC metals exhibit a typical ductile behavior featured by marked [plastic deformation](#) and dimpled rupture surface. In contrast to this, at [low temperatures](#), they generally fail by cleavage characterizing completely brittle behavior. A common criterion is to associate the [transition temperature](#) with the temperature at which the fracture is characterized by 100% cleavage. Three basic factors contribute to a brittle-cleavage type of fracture. They are: (i) a triaxiality of the stress state, (ii) a low temperature, and (iii) a [high strain rate](#) or rapid rate of loading. In the present work, the first factor is controlled by the shape of the notch, the temperature varies in the range of ductile-to [brittle transition](#) and the high strain rate is ensured by the dynamic [Charpy testing method](#). Data in [Table 2](#) confirm that the stress distribution influences strongly the toughness behavior: the increase in the [notch tip](#) radius leads to a significant increase in fracture toughness. The AE response was characterized by the change in the AE energy released during impact bending. Let us note it once again that the signal represented in [Fig. 1](#) was recorded in the [continuous mode](#). This signal is

synchronized with the  $dF/dt$  curve to establish the correlation between two primary stages of [impact loading](#) and the AE signal. The AE envelope varies considerably making it possible to reveal the sub-stages during impact loading, c.f. [\[33\]](#). [Quantitative measurements](#) of the [absolute values](#) of AE [energy release](#) associated with the dynamic source is both mathematically formidable and experimentally challenging. It requires solution of an [inverse problem](#), where an *a-priori* unknown [transfer function](#) should be found experimentally with high accuracy as it is done for example in [\[34\]](#), [\[35\]](#). Considering the complexity of experimental setup, quantitative source [characterization](#) is extremely challenging and therefore it was not performed in the present work. Since only relative measurements were made, the AE energy is expressed in arbitrary units unlike expended [energy measured](#) conventionally in [Joules](#).



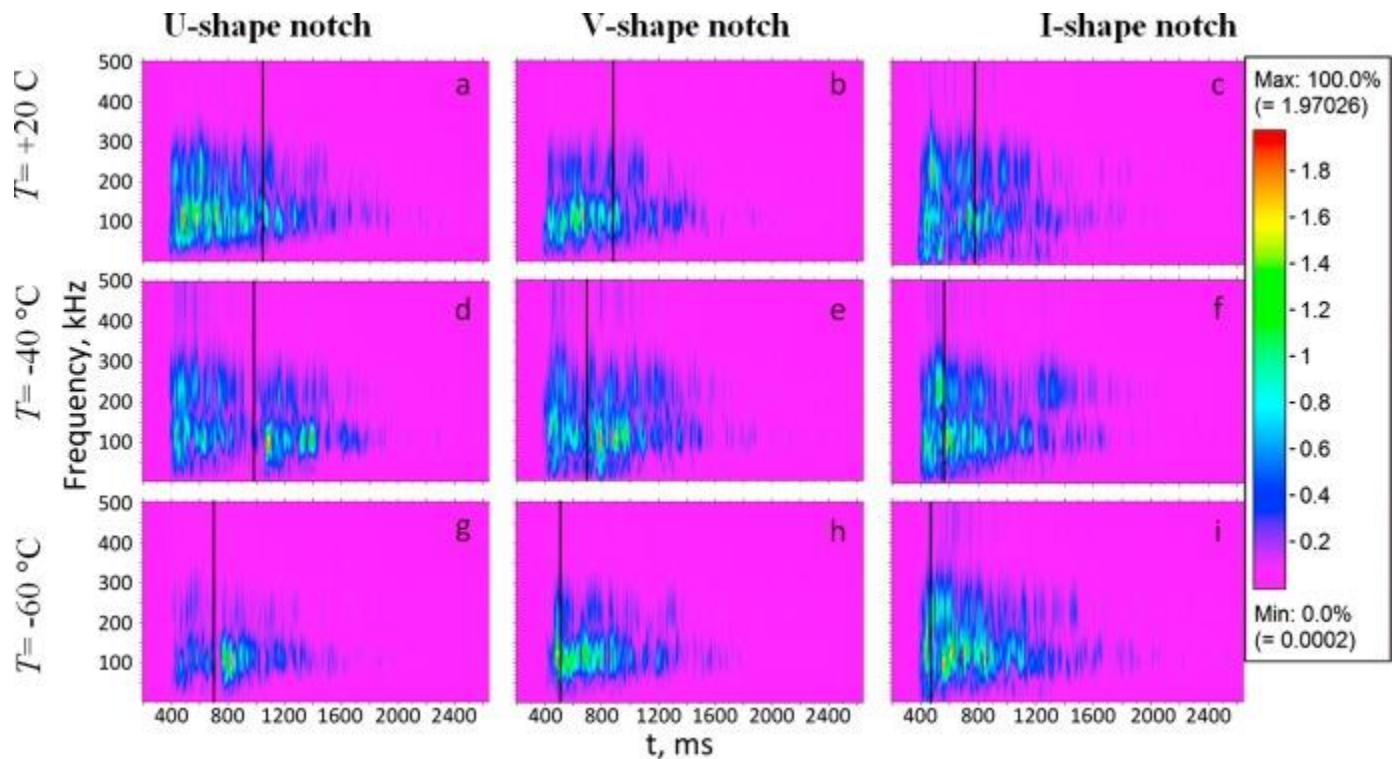
1. [Download high-res image \(651KB\)](#)
2. [Download full-size image](#)

Fig. 1. Time dependence of the [loading parameters](#)  $F(t)$  and  $dF(t)/dt$  synchronized with AE envelope obtained during dynamic [Charpy](#) testing of the specimens with different notch shapes at  $T = +20\text{ }^{\circ}\text{C}$  (a–c),  $-20\text{ }^{\circ}\text{C}$  (d–f), and  $-60\text{ }^{\circ}\text{C}$  (g–i). The dashed lines separate the stages of [crack initiation and propagation](#), which have been identified according to the ASTM procedure by analyzing the loading diagrams.

Table 2. Expended [mechanical energy](#)  $E_{\text{exp}}$  and released AE energy  $E_{\text{rel}}$  in impact bending of 17Mn1Si steel during stage I/stage II (and their ratios) at different test temperatures.

$T, \text{ }^{\circ}\text{C}$	$E_{\text{exp}}, \text{ J}$	$E_{\text{rel}}, \text{ a.u.}$	$E_{\text{exp}}, \text{ J}$	$E_{\text{rel}}, \text{ a.u.}$	$E_{\text{exp}}, \text{ J}$	$E_{\text{rel}}, \text{ a.u.}$
	U-notch		V-notch		I-notch	
+20	37.6/43.2 (0.87)	0.40/0.22 (1.81)	27.4/30.1 (0.91)	0.14/0.09 (1.55)	21.1/34.0 (0.62)	0.04/0.05 (0.80)
-20	38.8/12.8 (3.03)	0.09/0.12 (0.82)	18.3/18.0 (1.02)	0.07/0.17 (0.41)	7.7/30.3 (0.25)	0.03/0.11 (0.27)
-60	20.2/4.8 (4.21)	0.07/0.20 (0.35)	2.57/4.8 (0.54)	0.04/0.34 (0.12)	2.1/5.3 (0.40)	0.02/0.22 (0.09)

[Fig. 2](#) shows the wavelet time-frequency representation of AE signals during [dynamic fracture](#). The dashed line separates the stages of [crack initiation and propagation](#) identified according to the ASTM procedure [\[25\]](#) by analyzing the loading diagrams. A visual comparison of provided data reveals that the [major part](#) of the “energy” of the wavelet spectrum shifts towards stage II when the test temperature decreases and the [brittle fracture](#) component increases. This tendency is most pronounced for the specimens with the blunt U-notch, [Fig. 2a, d, g](#). During impact bending at room temperature when fracture toughness is relatively high, the amount of energy expended at first and second fracture stages, is comparable. Nevertheless, when the ductile crack initiates at stage I a considerable mechanical work is required. Therefore, the released [elastic energy](#) is somewhat higher at this stage. At the lowest temperature, the fracture is almost brittle and the energy is mostly released during crack propagation. The brittle [crack growth](#) is usually accompanied by the high power AE [transients](#) which are clearly seen in the wavelet spectra at low temperatures. That is why the amount of energy (per unit time) at the crack propagation stage is higher than in stage I at temperatures below ambient. For the sharpest I-notch, the AE [waveform](#) and the wavelet spectrum varies to a much [lesser extent](#) for all three test temperatures, [Fig. 2, c, f, i](#). Overall, comparing [Fig. 1, Fig. 2](#) one can see that while the AE envelopes look similar for different tests, the wavelet representation shows that the onset of stage II depends on the notch shape and temperature.



1. [Download high-res image \(471KB\)](#)
2. [Download full-size image](#)

Fig. 2. Wavelet spectrum of the AE signal corresponding to impact fracture of specimens with different notch shapes (a,d,g – U-notch; b,e,h, – V-notch; c,f,i – I-notch) tested at  $T = +20\text{ }^{\circ}\text{C}$  (a–c),  $-20\text{ }^{\circ}\text{C}$  (d–f), and  $-60\text{ }^{\circ}\text{C}$  (g–i). The vertical lines delineate two stages of crack evolution in the same way as shown in [Fig. 1](#).

The values of the [mechanical energy](#) expended during fracture and the elastic energy released in the AE form were analyzed using the [dynamic loading](#) curves and the accompanying AE signals for initiation and propagation stages separately. The ratio of the elastic energy released at these two stages for both the sharpest and the bluntest notch also tends to change depending on the [stress concentration](#), see [Table 2](#). For the U-notched specimen, this ratio is two times higher during stage I than during stage II at room temperature, while for the I-notched specimen the released AE energy is almost equally distributed between both stages. On the other hand, for the U-notched specimen, the energy released during stage II at  $T = -60\text{ }^{\circ}\text{C}$  is about 2.8 times higher than that during stage I. For the sharpest I-notched specimen this ratio is over 8. These observations show that when the fracture toughness drops due to cold [embrittlement](#), the release of elastic energy associated with AE during crack propagation tends to increase and prevails over that during [crack initiation](#). Lowering the temperature impedes plastic deformation and increases the contribution from [cleavage fracture](#) to

the overall [fracture behavior](#) and specifically to the released energy (the latter is known to increase with the increasing size of cleavage facets, e.g. see a theoretical background developed in [\[36\]](#), [\[37\]](#) and experimental evidence provided in [\[38\]](#). Besides, the increasing [brittleness](#) in the fracture behavior is inexorably associated with the increasing rate of remaining plastic deformation until the latter completely vanishes below [nil ductility temperature](#). As the AE power (energy) is linearly proportional to the [plastic strain rate](#) [\[39\]](#), this contribution cannot be disregarded as long as the completely brittle fracture is observed.

The [fracture energy](#) determined from the impact toughness curve (“expended energy” –  $E_{\text{exp}}$ ) is expressed in Joules, and the energy estimated from the AE envelope (“released energy” –  $E_{\text{rel}}$ ) is in arbitrary units. These quantities are summarized in [Table 2](#) for different specimens and temperatures.

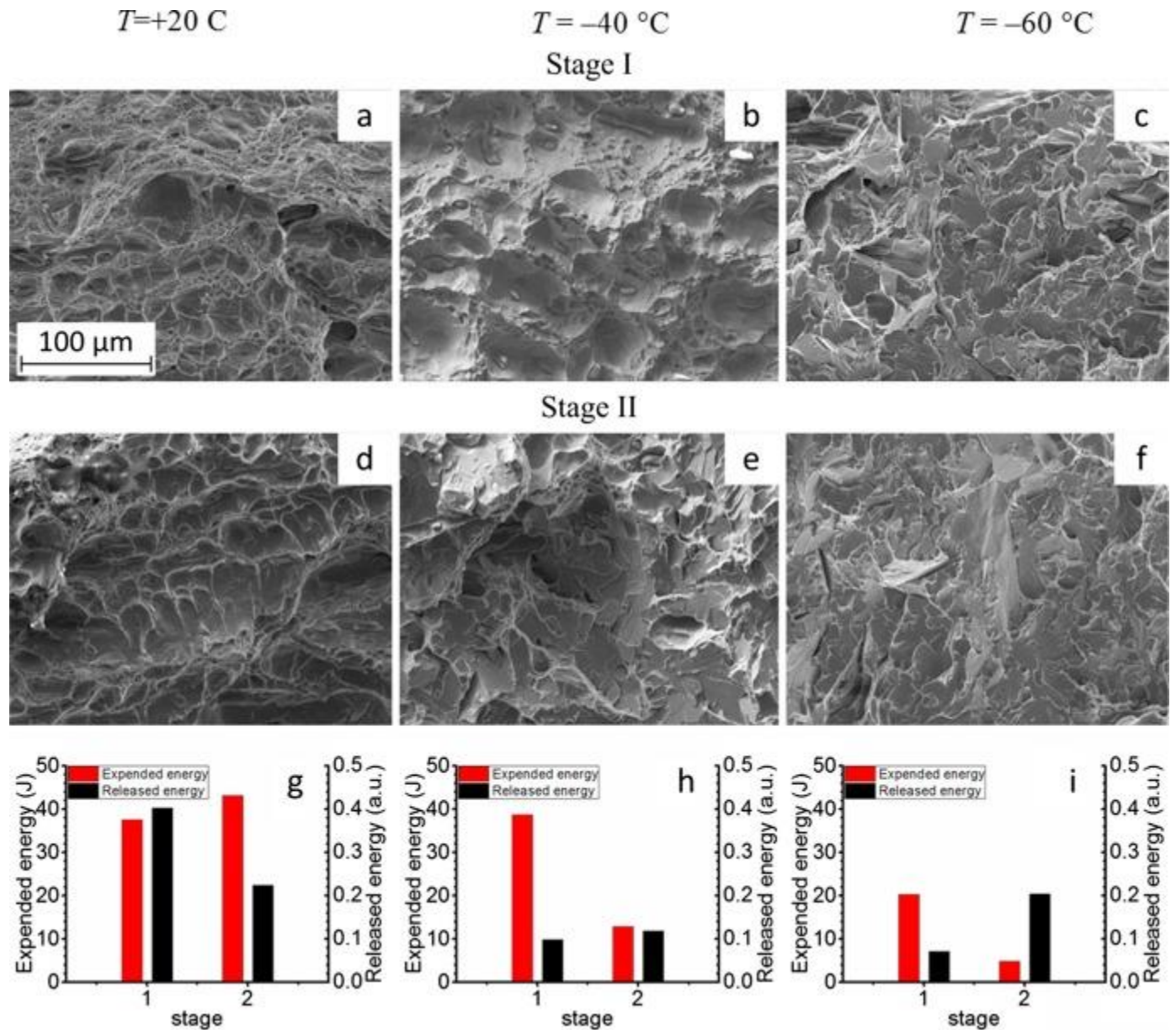
### 3.1. U-notch

**$T = +20\text{ °C}$**  (the most [ductile fracture](#) behavior, the critical fracture toughness  $KCU_{+20\text{ °C}} = 106\text{ J/cm}^2$ ). The analysis of data shown in [Fig. 1](#) reveals that the maximum AE energy corresponds to the initial loading stage before the load reaches its maximum  $P_{\text{max}}(t < 1.08\text{ ms})$ . This is in good agreement with the AE envelope shape. The subsequent transition from the crack initiation stage to the stage of propagation is accompanied by a decrease in the recorded AE signal. This indicates that the dissipation of the elastic energy imposed into the Charpy specimen during ductile fracture on stage II is mainly associated with the [heat release](#) due to [dislocation mechanisms](#) of plastic deformation. The crack initiation resistance is overcome on stage I with a large energy release (cf.  $E_{\text{relI}} = 0.4\text{ a.u.}$ ,  $E_{\text{relII}} = 0.22\text{ a.u.}$ ). Concurrently, the fracture energies at both stages are comparable (cf.  $E_{\text{expI}} = 37.6\text{ J}$ ,  $E_{\text{expII}} = 43.2\text{ J}$ ), which is most probably caused by a relatively [long time](#) of crack propagation.

**$T = -20\text{ °C}$**  ( $KCU_{-20\text{ °C}} = 51.6\text{ J/cm}^2$ ). Compared to room temperature testing, [Fig. 1d](#) shows that the fracture behavior tends to be more brittle. The shape of the impact toughness curve resembles that observed at room temperature. However, the maximum AE energy corresponds to the load beyond  $P_{\text{max}}(t > 1.01\text{ ms})$ , which is also seen in the AE wavelet spectrum, [Fig. 2d](#). Similarly to testing at room temperature, the largest fraction of AE energy is produced in the frequency range of 50–150 kHz. The amount of energy released during stage I decreased by 10 a.u. compared to that measured at 20 °C. However, during crack propagation, the same parameter increased by approximately 20 a.u. (cf.  $E_{\text{relI}} = 0.09\text{ a.u.}$ ,  $E_{\text{relII}} = 0.12\text{ a.u.}$ ). Thus, the more brittle fracture behavior during stage II was accompanied by a significant increase in the released

energy. This is consistent with the fact that the fracture energy at the second stage (more brittle) was almost four times lower than in the first stage (more ductile) (cf.  $E_{\text{expI}} = 38.8 \text{ J}$ ,  $E_{\text{expII}} = 12.8 \text{ J}$ ). Compared to room temperature testing, the amount of the released AE energy during the crack initiation stage changed appreciably although the approximately equal amount of the mechanical energy was expended on the same stage. This means that the AE energy and the mechanical energy are not related unambiguously and further work is still needed to establish such a relation firmly.

**$T = -60 \text{ }^\circ\text{C}$**  ( $\text{KCU}_{-60^\circ\text{C}} = 32 \text{ J/cm}^2$ ). [Fig. 1g](#) shows the results of testing at the lowest temperature below the ductile-to-brittle transition. The brittle fracture behavior is evident from the impact loading curve. The maximum AE energy is again seen at loads beyond  $P_{\text{max}}$ , i.e., during stage II ( $t > 0.75 \text{ ms}$ ). The AE energy at the crack initiation stage is almost three times lower than at the propagation stage (cf.  $E_{\text{relI}} = 0.07 \text{ a.u.}$ ,  $E_{\text{relII}} = 0.20 \text{ a.u.}$ ). In comparison with the results of testing at  $T = -20 \text{ }^\circ\text{C}$ , the amount of energy released at the crack initiation stage decreased more than twice, while during stage II it remained almost unchanged. Thus, the [brittle crack](#) propagation was systematically accompanied by a [high energy](#) AE: the greater the brittleness, the higher the AE. This agrees well with the fracture energy estimates (cf.  $E_{\text{expI}} = 20.2 \text{ J}$ ,  $E_{\text{expII}} = 4.8 \text{ J}$ ). The test temperature did not affect the characteristic AE frequency range significantly, [Fig. 2f](#). For the sake of comparison, the [energy values](#) characterizing the impact fracture behavior are represented in [Fig. 3](#) together with typical SEM [micrographs](#) of [fracture surfaces](#) for both stages.



1. [Download high-res image \(869KB\)](#)
2. [Download full-size image](#)

Fig. 3. Morphology of [fracture surface](#) and characteristic energy parameters for [crack initiation](#) (I) and propagation (II) stages calculated from the [dynamic loading](#) curve (red) and from AE data (black) for U-notched [specimens tested](#) at +20 °C (a, d, g), -20 °C (b,e,h), and -60 °C (c,f,i). (For interpretation of the references to color in this figure legend, the reader is referred to the web version of this article.)

Thus, the decreasing test temperature results in a gradual decrease of the amount of the expended mechanical energy and of the AE released during stage I crack initiation.

On the other hand, the amount of the mechanical energy expended during stage II crack propagation also gradually decreases, while the AE energy increases.

### 3.2. V-notch

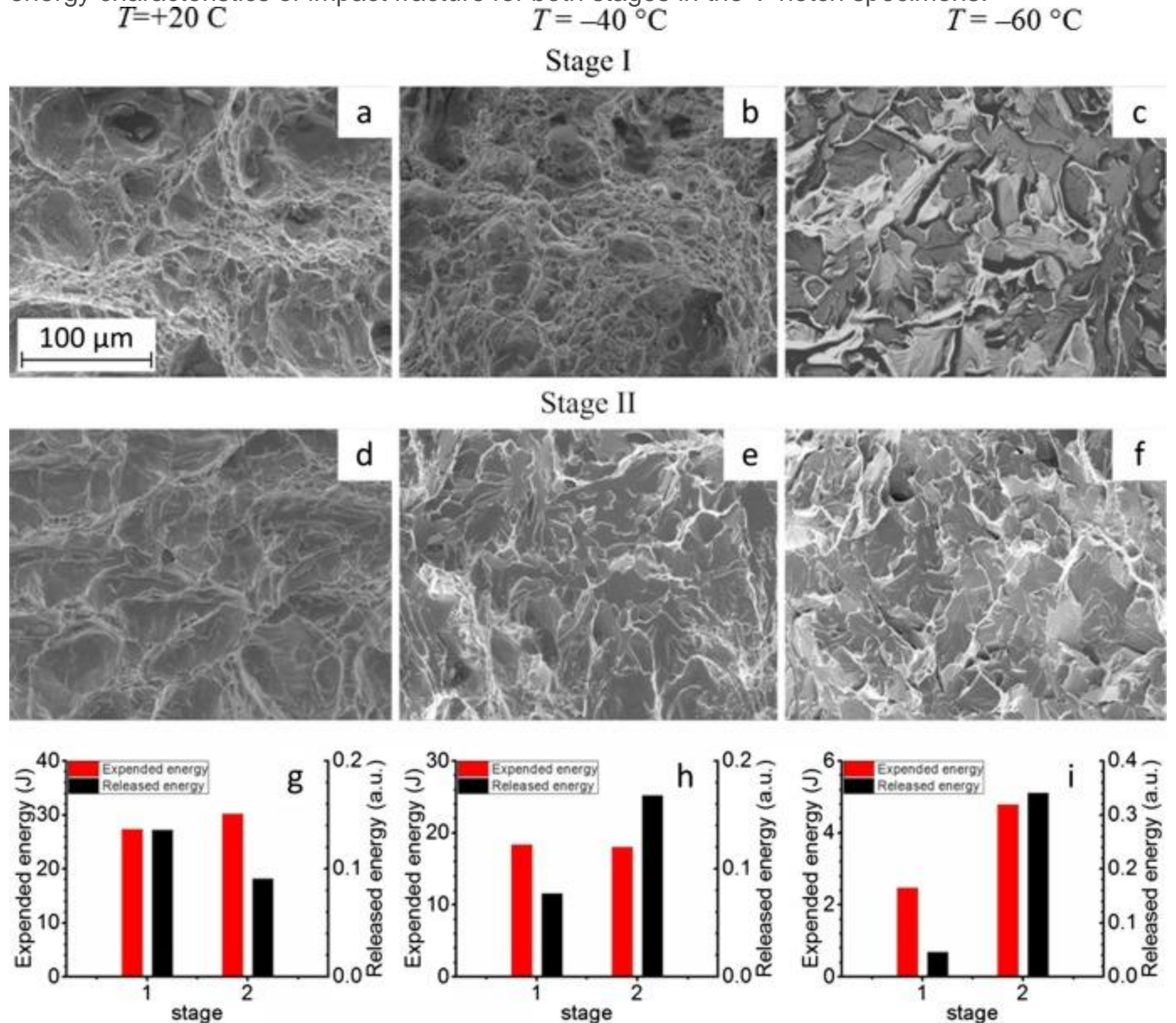
**T = +20 °C.** A decrease in the notch tip radius leads to an increase in the [stress concentration factor](#). It should also contribute to the increase in the brittle fracture component (especially at the initiation stage I). [Fig. 1b](#) shows the results of room temperature testing of the specimens exhibiting the most ductile fracture behavior for the given notch shape (the fracture toughness  $KCV_{+20^{\circ}\text{C}} = 73.3 \text{ J/cm}^2$ ). Similarly to the U-notched [specimen tested](#) at the same temperature, the maximum AE energy is observed at the load lower than  $P_{\text{max}}$  ( $t = 0.92 \text{ ms}$ ), which also agrees well with the AE envelope shape, [Fig. 2b](#). The  $KCV$  value decreased by more than  $30 \text{ J/cm}^2$  if compared to the  $KCV$  value of the specimen tested at the same temperature. However, in the case of the [sharper notch](#), the ratio of the fracture energy during stages I (cf.  $E_{\text{expl}U} = 37.6 \text{ J}$ ,  $E_{\text{expl}V} = 27.4 \text{ J}$ ) and II remained almost the same (cf.  $E_{\text{expl}U} = 43.2 \text{ J}$ ,  $E_{\text{expl}V} = 30.1 \text{ J}$ ). Apparently, for this reason, the transition from the crack initiation stage to the crack propagation stage is accompanied by a decrease in the AE energy (cf.  $E_{\text{rel}I} = 0.14 \text{ a.u.}$ ,  $E_{\text{rel}P} = 0.09 \text{ a.u.}$ ). On the other hand, the fracture energy corresponding to each stage is comparable.

**T = -20 °C.** Results of testing at this temperature are shown in [Fig. 1d](#). The fracture occurs in a more brittle mode ( $KCV_{-20^{\circ}\text{C}} = 46 \text{ J/cm}^2$ , which, however, is only by of  $5 \text{ J/cm}^2$  lower than the fracture toughness of the U-notched specimen). The shape of the dynamic loading curve is again similar to that for room temperature tests. The maximum AE energy is seen after the maximum load  $P_{\text{max}}$  ( $t = 0.72 \text{ ms}$ ), like that in the U-notched specimen. This is also seen in the wavelet spectrum of the AE signal, [Fig. 2e](#). The fracture energies during both stages I and II were approximately equal, unlike those for the U-notched specimen (cf.  $E_{\text{expl}I} = 18.3 \text{ J}$ ,  $E_{\text{expl}II} = 18.0 \text{ J}$ ). On the other hand, as compared to the U-notch, the amount of the released energy at stage I decreased considerably, while during stage II it increased only slightly.

**T = -60 °C.** In contrast to tests on the U-notched specimen, the fracture of the V-notched specimen was almost brittle at  $-60^{\circ}\text{C}$  ( $KCV_{-60^{\circ}\text{C}} = 9.3 \text{ J/cm}^2$ ). The embrittlement affected both the shape of the impact loading curve and the duration of the characteristic stages, [Fig. 1h](#). For this reason, the maximum AE energies correspond to the load range both before and mostly after reaching  $P_{\text{max}}$ . Moreover, the brittle fracture behavior during stage II is reflected in the AE [signal/spectrum](#) shape, [Fig. 2h](#), even at the time when the [external load](#) dropped. The brittle fracture behavior is also in good

agreement with the low fracture energies measured (cf.  $E_{\text{expI}} = 2.47 \text{ J}$ ,  $E_{\text{expII}} = 4.79 \text{ J}$ ). Compared to the U-notched specimen, the amount of the released energy during stage I decreased by a factor of three. However, it remained almost unchanged during the propagation stage (cf.  $E_{\text{relI}} = 0.04 \text{ a.u.}$ ,  $E_{\text{relP}} = 0.34 \text{ a.u.}$ ).

[Fig. 4](#) shows typical SEM micrographs of the fracture surfaces and compares the energy characteristics of impact fracture for both stages in the V-notch specimens.



1. [Download high-res image \(800KB\)](#)
2. [Download full-size image](#)

Fig. 4. Morphology of [fracture surface](#) and characteristic energy parameters for [crack initiation](#) (I) and propagation (II) stages calculated from the [dynamic loading](#) curve (red)

and from AE data (black) for V-notched [specimens tested](#) at +20 °C (a, d, g), -20 °C (b,e,h), and -60 °C (c,f,i). (For interpretation of the references to color in this figure legend, the reader is referred to the web version of this article.)

Thus, these findings corroborate the thesis that the more brittle fracture behavior is accompanied by a higher-energy AE signal. It should also be highlighted that the AE energy released during the initiation stage I decreases significantly if compared to the U-notched specimen. However, only small relative change is noticed during stage II. It has been shown that the increase in the stress concentration factor at the notch tip of Charpy specimens and the test temperature reduction is accompanied by a decrease in the amount of the mechanical energy expended during crack initiation and propagation, as compared to that in the U-notched specimens, while the amount of (normalized) AE released energy remains approximately the same.

### 3.3. I-notch

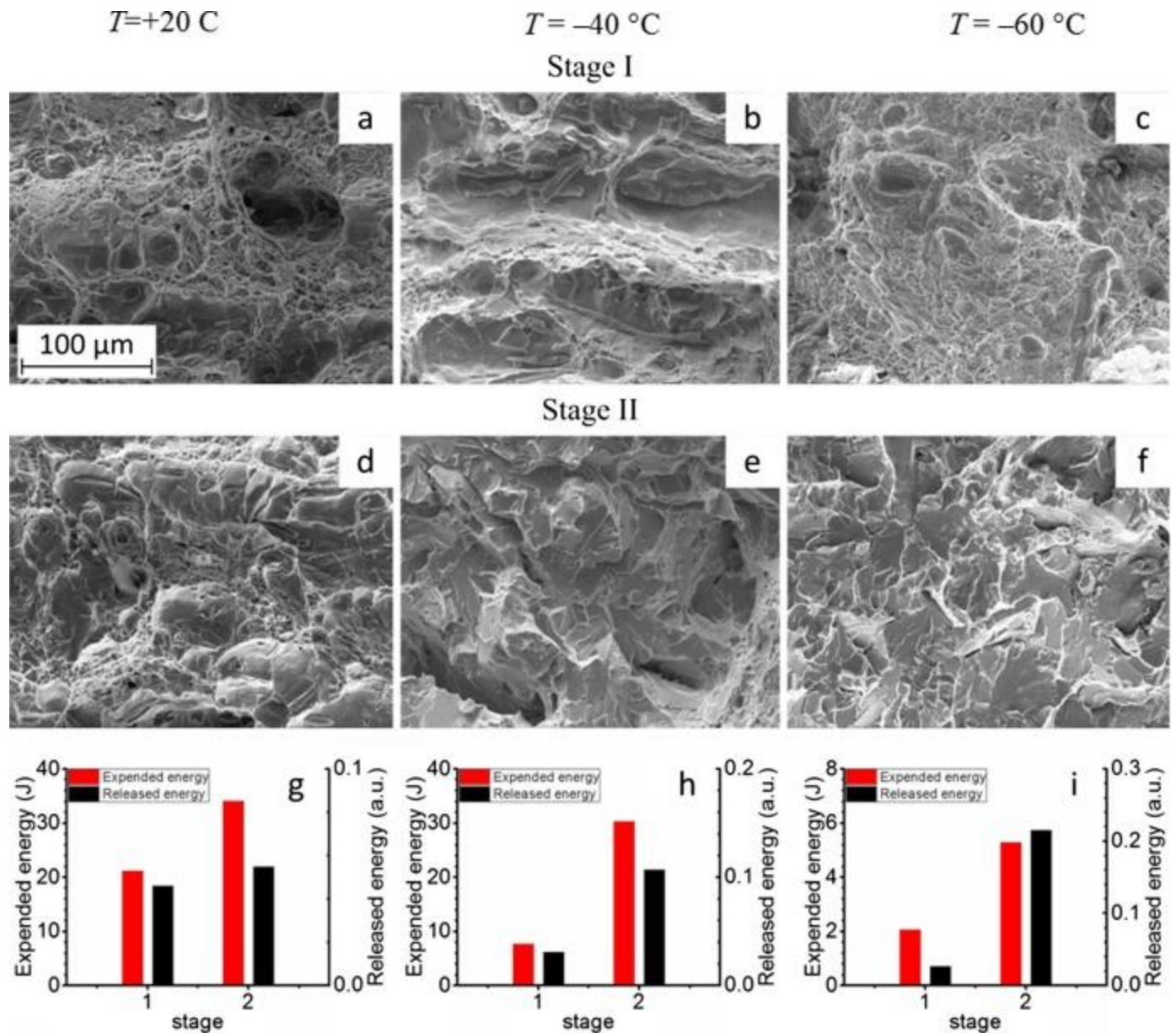
**$T = +20\text{ °C}$ .** Reduction in the notch tip radius increases the stress concentration and promotes brittle fracture, which is particularly pronounced during the initiation stage I. [Fig. 1c](#) shows the testing results for specimen loaded at room temperature. The fracture toughness  $K_{IC|+20\text{ °C}} = 70\text{ J/cm}^2$  is found to be close to that for the V-notched specimen. Similarly to the U- and V-notched specimens, the maximum AE energy is noticed at loads smaller than  $P_{\max}(t < 0.81\text{ ms})$ , which is again nicely seen in the wavelet spectrum of the AE signal, [Fig. 2c](#). In contrast to the less sharp V-notch, there is only a little difference in the fracture energy values measured during the first and the second stages, [Table 2](#). Evidently, it is the shorter duration of stage I and the smaller amount of fracture energy in the specimen with the sharpest notch at this stage that caused a comparable level of AE energy in both stages I and II (which is different from the behavior of the U- and V-notched specimens tested at room temperature).

Nevertheless, the amount of the released energy in the I-notched specimen during stage II is highest compared to other notches.

**$T = -20\text{ °C}$ .**[Fig. 1f](#) represents the results for the V-notched specimen tested at -20 °C. The brittle fracture component increased and the fracture toughness reduced reasonably to  $K_{IC|-20\text{ °C}} = 38\text{ J/cm}^2$ , which is by approximately  $8\text{ J/cm}^2$  smaller than that for the V-notched specimen. The shape of the impact loading curve having only one maximum is no longer similar to that obtained at room temperature [impact testing](#). Compared to specimens with other notch shapes, the AE energy [peak shifts](#) further to shorter loading times. The AE maximum is attained before the  $P_{\max}(t < 0.56\text{ ms})$  value is

reached (see also the AE wavelet spectrum shown in [Fig. 2f](#)). The amount of AE energy measured during stage II of the crack growth is still significant (cf. for the I-notched specimen  $E_{relI} = 0.03$  a.u.,  $E_{relII} = 0.11$  a.u.). Compared to the room temperature test, the value of this parameter decreased almost twice for stage I, while for the crack propagation stage II it increased almost 1.5 times. The fracture energy was found to be more than twice as large as that during stage I, similarly to the V-notch in stage II.  **$T = -60$  °C.** The fracture at this temperature was almost brittle resembling that in the V-notched specimen. The fracture toughness was estimated as  $KIC_{-60\text{ °C}} = 9.4$  J/cm<sup>2</sup>. Therefore, both the shape of the dynamic loading curves and the characteristic fracture stages are similar to those in the V-notched specimen, [Fig. 1i](#). In contrast to room temperature testing, the position of the maximum AE energy is observed beyond  $P_{max}(t > 0.4$  ms). Similarly to the V-notched [specimen tests](#) at the same temperature, the brittle fracture behavior during stage II is recognized in the AE wavelet spectrum, [Fig. 2i](#). The released AE energy during stage I is substantially less than that during stage II (cf.  $E_{relI} = 0.02$  a.u.,  $E_{relII} = 0.22$  a.u.). Furthermore, it reduced appreciably in comparison to that obtained at  $T = -20$  °C. In comparison with the V-notched specimen, only the energy released on stage II increased noticeably (by more than 10 a.u.). The brittle fracture behavior results in low mechanical energies estimates (cf.  $E_{expI} = 2.06$  J,  $E_{expII} = 5.29$  J). Although the fracture energy value during stage II is only of 2.5 times larger than during stage I, the AE energy emitted during the stage of crack propagation is almost by order of magnitude higher than that during stage I. Thus, the fracture energy ratio  $E_{expII}/E_{expI}$  does not necessarily [correlate](#) with the respective ratio of the AE energy.

The results obtained on the I-notched specimen tests are summarized in [Fig. 5](#) showing both the SEM images of the typical fragments of the fracture surface observed during both crack initiation and propagation stages and corresponding AE energies. Overall, the observed [experimental findings](#) related to the change in the mechanical energy expended and released during fracture of Charpy specimens with [decreasing temperature](#) are qualitatively similar for the specimens with V- and I-notches, though they are not quantitatively identical.



1. [Download high-res image \(834KB\)](#)
2. [Download full-size image](#)

Fig. 5. Morphology of [fracture surface](#) and characteristic energy parameters for [crack initiation](#) (I) and propagation (II) stages calculated from the [dynamic loading](#) curve (red) and from AE data (black) for I-notched [specimens tested](#) at +20 °C (a, d, g), -20 °C (b,e,h), and -60 °C (c,f,i). (For interpretation of the references to color in this figure legend, the reader is referred to the web version of this article.)

Experimental data concerning the expended mechanical energy and the released AE energy measured during impact testing represented in [Table 1](#) and [Fig. 3](#), [Fig. 4](#), [Fig. 5](#) reveal systematic trends in the behavior of the [mechanical impact](#) fracture energy and

the AE energy depending on the notch shapes and temperatures. For the crack initiation stage one can see that the lower the temperature is, the lower both [energy components](#) are. A different trend is observed at the crack propagation stage: the expended mechanical energy decreases with decreasing temperature, but the fraction of the released AE energy increases. This result can be rationalized as follows. The ductile fracture mode dominates during the initiation stage I. The ductile behavior is mediated by dislocations whose activity generates measurable AE. However, the AE energy (or power) associated with [dislocation motion](#) is low compared to that during initiation and propagation of a brittle crack. Temperature reduction strongly reduces the thermally-activated dislocation activity, which is particularly clear in BCC metals, alloys, and steels. During crack propagation, especially at low temperatures, a smaller amount of energy is expended for damping due to plastic deformation, and therefore the fraction of the released energy is higher.

In summary, the following remarks are in place. In line with existing findings, e.g. [\[28\]](#), [\[40\]](#), salient results obtained from the [present investigation](#) demonstrate that AE responds remarkably differently to brittle and ductile fracture during ductile-to-brittle transition in dynamic testing of plan [carbon steels](#). While the simplistic approaches employing the AE counts [\[28\]](#), [\[40\]](#) can be efficient for crack initiation during brittle fracture by the jump-like behavior of the cumulative AE counts, the [energetic](#) characteristics of the AE signal and their spectra also need to be considered to monitor the fracture behavior during ductile fracture (c.f. [\[24\]](#)). The expended mechanical energy shows a typical decreasing trend during both stage I (initiation) and II (propagation) fracture with cold embrittlement. The released AE energy however exhibits different trends on two stages with temperature reduction – it reduces concomitantly with the [expended energy](#) during stage I when temperature reduces, but, as opposes to the expended energy, it tends to increases during stage II. Unlike the cited works [\[28\]](#), [\[40\]](#) employs the AE [energy analysis](#) during Charpy impact testing. Chuluunbat et al. [\[24\]](#) used the [Fourier spectral decomposition](#) to reveal the differences in the AE signals during different stages of fracture evolution. Although, some correlation between the AE frequency, [amplitude](#) and [defect size](#) were reported, the present authors did not find any rationale in using the Fourier analysis for strongly transient AE data. Tronskar et al. [\[23\]](#) employed a [short-time Fourier transform](#) to highlight the difference between the stage I and stage II AE transients. The efficiency was demonstrated of the time-frequency analysis for detection of ductile tearing initiation and for distinction between different [failure modes](#). In the present work, the wavelet spectral representation was shown for the released energy visualization at

various stages. The proposed analysis can be regarded as suitable for providing a [measure](#) of both brittle and ductile fracture initiation toughness at different temperatures for engineering [fracture mechanics](#), provided the appropriate calibration of the AE technique is utilized. The investigation conducted has shown that a remarkable scatter can be expected. Hence, even though the trends in the AE behavior are clearly seen and the correlation between expended and released energies is deemed important for further development of instrumented fracture mechanics testing, it is premature to speak about quantitative relationships between AE and fracture mechanics parameters. A relatively [large number](#) of tests is required for calibration and establishing the sought quantitative relationships (this will be the scope of the future work). This scatter is supposed to be caused by material heterogeneity, notch geometry and method of notch manufacturing, and partly by [constraint effects](#).

As a final note, the significant drop in fracture toughness in the lower shelf [temperature region](#) is critical for ductile low-carbon ferrite-perlite steels widely used for [structural applications](#) in [cold climate](#). Being representative of a class of ductile [pipe steels](#) the studied commercial 17Mn1Si steel exhibits a typical ductile-to-brittle transition behavior in the range of service temperatures. Without any limitation, the results can be extended to the whole class of [structural steels](#) and the proposed methodology of AE signal analysis during dynamic testing applies to other steels of this kind.

## 4. Conclusions

The impact [fracture behavior](#) of ductile 17Mn1Si [pipe steel](#) with different notch shapes was investigated during testing at different temperatures between +20 °C to -60 °C covering the range of ductile-to-brittle transition. The analysis was performed by comparing the [energy expended](#) in [crack initiation and propagation](#) according to the [dynamic loading](#) curve and the released AE energy in all cases. The [energy distribution](#) of AE signals accompanying impact fracture was investigated in the time-frequency domain by continuous wavelets revealing a distinction between [main stages](#) of fracture development. In short, the results are summarized as following.

### 4.1. U-notched specimens

A typical trend with decreasing test temperature is seen as a gradual decrease in the amount of expended and released energy during stage I. The amount of expended energy during stage II also gradually decreases, while the amount of AE energy increases.

### 4.2. V-notched specimens

The fracture behavior is more brittle with an appreciably larger amount of the released AE energy than that in the U-notched specimens. Compared to the U-notched specimen, there is a noticeable decrease in the AE energy released during the stage I fracture, while during stage II it changes only slightly.

#### 4.3. I-notched specimens

The behavior of expended and released [energy components](#) during fracture of the V- and I-notched specimens is qualitatively similar (though not identical) because their [crack tip](#) radii are similar and the [brittle fracture](#) dominates in both specimens. Both the expended [mechanical impact](#) energy and the released AE energy exhibit similar trends during the [crack initiation](#) stage: the lower the temperature, the lower the energy regardless of the notch geometry. A significantly different behavior is observed during the crack propagation stage: while the expended energy decreases with temperature similarly to that on stage I, the released energy, on the contrary, increases appreciably.

There is still a lot of room for optimization of all elements in the AE acquisition-processing chain. This concerns (i) the [sensor type](#) and its location; (ii) a way of a time–frequency representation of a signal; (iii) a process of information squeezing to physically and mechanically justifiable criteria, etc. A radical departure is needed in this way from qualitative correlations to causation and quantitative relations between the measurable parameters of [fracture mechanics](#) and AE characteristics. The progress in this direction is anticipated through a thorough constitutive (possibly [multiscale](#)) [modeling](#) of [dynamic fracture](#) in conjunction with microstructural processes underlying both brittle and ductile fracture and their interactions.